Water Research 193 (2021) 116880

Contents lists available at ScienceDirect

Water Research

journal homepage: www.elsevier.com/locate/watres

Fluoride release from carbonate-rich fluorapatite during managed aquifer recharge: Model-based development of mitigation strategies

David Schafer[a,b,c], Jing Sun[a,d], James Jamieson[a,b], Adam Siade[a,b,c], Olivier Atteia[e], Simone Seibert[f], Simon Higginson[g], Henning Prommer[a,b,c,*]

[a] University of Western Australia, School of Earth Sciences, Crawley WA 6009, Australia
[b] CSIRO Land and Water, Private Bag No. 5, Wembley, WA 6913, Australia
[c] National Centre for Groundwater Research and Training, Adelaide, GPO Box 2100, SA 5001, Australia
[d] State Key Laboratory of Environmental Geochemistry, Institute of Geochemistry, Chinese Academy of Sciences, Guiyang, 550081, China
[e] ENSEGID, Université de Bordeaux, 1 Allee Daguin, 33607 Pessac Cedex, France
[f] Federal Institute for Geosciences and Natural Resources, Hannover, Germany
[g] Water Corporation of Western Australia, PO Box 100, Leederville, WA 6902, Australia

ARTICLE INFO

Article history:
Received 19 November 2020
Revised 23 January 2021
Accepted 25 January 2021
Available online 28 January 2021

Keywords:
Fluoride
Managed aquifer recharge
Reactive transport modelling
CFA
Water treatment

ABSTRACT

Fluoride-bearing apatite minerals such as fluorapatite (FAP: $Ca_{10}(PO_4)_6F_2$) and related carbonate-rich fluorapatites (CFA: $Ca_{10}(PO_4)_5(CO_3,F)F_2$), which occur ubiquitously as trace components of rocks and sediments, may act as sources for geogenic groundwater fluoride contamination. CFA dissolution often occurs in conjunction with declining dissolved calcium concentrations. Therefore, managed aquifer recharge (MAR) operations using deionised or low calcium source water are at risk of disturbing the naturally persisting geochemical equilibrium between CFA and the ambient groundwater and induce fluoride mobilisation. In this study, we employ reactive transport modelling to investigate how an engineered manipulation of the MAR source water composition might mitigate such groundwater fluoride contamination. Based on a previously developed and calibrated model for Australia's largest groundwater replenishment operation, we investigate the efficiency of (i) raising aqueous calcium concentration through the addition of $CaCl_2$ or $Ca(OH)_2$ amendment, (ii) raising aqueous sodium concentrations through the addition of NaCl or sea salt amendment and (iii) raising the pH. The modelling results illustrate in detail how the geochemical zonation around injection boreholes evolves over time and how this affects fluoride release and attenuation for the different amendment types. Treatments involving the addition of calcium and sodium in the source water are both found to be effective at reducing maximum groundwater fluoride concentrations during MAR, with calcium generally producing the greatest reduction in maximum fluoride concentrations. In contrast, increasing the injectate pH was found to be inefficient in reducing fluoride concentrations significantly due to the strong pH buffering effect of the aquifer sediments.

1. Introduction

Increasing water demands and climate variability have caused aquifer depletion and seawater intrusion in Australia and elsewhere (CSIRO and BOM 2015; Fienen and Arshad 2016; UNESCO 2016). Managed aquifer recharge (MAR) is an increasingly used tool to combat these problems (Burris 2018; Casanova et al., 2016; Dillon et al., 2018; Ebrahim et al., 2016; Reichard and Johnson 2005). MAR involves the intentional infiltration or injection of various source water types into aquifers, often for later recovery (Dillon 2005; Dillon et al., 2018; Stefan and Ansems 2018). With recent advances and cost reductions in water treatment technology, reclaimed, highly treated wastewater has become an attractive source water type to supplement existing resources in many water scarce areas (Burris 2018; Casanova et al., 2016; Dillon et al., 2018; Ganot et al., 2018; Missimer et al., 2014; Reichard and Johnson 2005; Rodriguez et al., 2009; Stuyfzand et al., 2017). Compared to seawater desalinisation, wastewater recycling requires several additional advanced treatment steps such as ultraviolet light (UV) and ozonation to remove the significantly higher pathogen and contaminant loading (Yuan et al., 2019). Nevertheless, reclaimed wastewater is generally the economically more viable and environmentally more friendly option due to the often much lower salt

* Corresponding author.
E-mail address: Henning.Prommer@csiro.au (H. Prommer).

https://doi.org/10.1016/j.watres.2021.116880

load and energy consumption (Dillon et al., 2018; Missimer et al., 2014; Rodriguez et al., 2009; Zekri et al., 2014).

MAR of reclaimed wastewater plays a central role for indirect water reuse schemes as it provides a much needed additional treatment buffer, i.e., an aquifer where engineering risks and public perception issues preclude direct wastewater reuse (Dillon et al., 2018; Ganot et al., 2018; Gibson and Burton 2014; Ormerod 2015; Rodriguez et al., 2009; Wester et al., 2015; Wester 2016). However, the hydrochemical composition of the treated wastewater typically differs strongly from the native groundwater. MAR will therefore often trigger a pronounced geochemical disequilibrium within the target aquifer and induce various geochemical reactions between the injected water and the aquifer sediments. Previously reported water-sediment reactions observed during MAR include redox reactions, mineral dissolution, desorption of trace metals and metalloids, cation exchange and mobilisation of colloids (Brown and Misut 2010; Descourvieres et al., 2010; Fakhreddine et al., 2015; Fakhreddine et al., 2020; Ganot et al., 2018; Jones and Pichler 2007; McNab et al., 2009; Rathi et al., 2017; Treumann et al., 2014; Vandenbohede et al., 2013; Wallis et al., 2010). MAR with treated wastewater may induce additional, highly specific water-sediment interactions as a result of the very low concentrations of divalent cations (e.g., Ca^{2+} and Mg^{2+}), which are preferentially excluded during the reverse osmosis process compared to monovalent cations (Eisenberg and Middlebrooks 1985; Fakhreddine et al., 2015; Richards et al., 2011). Low concentrations of divalent cations in the recharged water have previously been shown to cause the release of adsorbed negatively charged contaminants during MAR by decreasing the density of positive surface charge on phyllosilicate clay minerals (Fakhreddine et al., 2015). Alternatively, they may trigger the enhanced dissolution of minerals such as calcite and dolomite of which divalent cations are a major component (Ganot et al., 2018; Vandenbohede et al., 2013). Those reactions may be exacerbated with low ionic strength injectant because divalent cations preferentially partition onto sediment exchanger sites relative to monovalent cations, thus increasing the degree of disequilibrium (Appelo and Postma 2005; Vandenbohede et al., 2013).

The long-term success of MAR schemes requires a thorough understanding of concomitant water-sediment interactions which may affect water quality or scheme operation. While ample attention has been given to the removal of contaminants prior to injection (Jokela et al., 2017; Yuan et al., 2019) as well as the potential for the aquifer to remove pathogens and dissolved organic pollutants (Betancourt et al., 2014; Händel and Fichtner 2019; Henzler et al., 2014; Kolehmainen et al., 2007; Kortelainen and Karhu 2006; Sidhu et al., 2015; Wiese et al., 2011), less attention has been given to a systematic optimisation of water treatment options to proactively prevent water-sediment interactions that release geogenic contaminants (Fakhreddine et al., 2021). In cases where the geochemical mechanisms that control the release of geogenic contaminants are well understood, mitigation strategies involving the targeted modification of the injectant composition through water treatment can be developed. For example, Prommer et al. (2018) demonstrated that pre-treatment involving deoxygenation could prevent pyrite oxidation and associated arsenic release during reinjection of co-produced water from coal seam gas production. Sun et al. (2020) showed through reactive transport modelling how changes in the water treatment processes affect long-term groundwater pH changes during groundwater replenishment with reclaimed wastewater. Also, Fakhreddine et al. (2015) investigated experimentally at the laboratory scale a series of amendments of divalent cations to deionised reclaimed water and how this would reduce the release of arsenate from phyllosilicate clay minerals in shallow aquifer sediments.

With the present study we systematically investigate how the release of fluoride, which can occur during the injection of low-ionic strength water, can be mitigated to identify possible water treatment options. At the selected study site the fluoride-bearing apatite mineral carbonate-rich fluorapatite (CFA: $Ca_{10}(PO_4)_5(CO_3F)F_2$) has been identified as a source of geogenic release of fluoride in response to replenishing the aquifer with highly purified wastewater (Schafer et al., 2018). Fluoride in aquifers used for drinking water abstraction needs to be closely monitored as both deficiency and excess of fluoride can lead to human and animal health problems (Brahman et al., 2013; Knappett et al., 2020). The World Health Organisation drinking-water quality guidelines considers that fluoride concentration <0.5 mg/L (<26 µM) is beneficial for human health while concentrations exceeding the guideline value of 1.5 mg/L (79 µM) may lead to health problems such as dental and skeletal fluorosis (WHO 2017). Excessive fluoride may also lead to learning difficulties in children (Yu et al., 2018). Here we use a process-based reactive transport modelling framework to provide deeper insights into the critical geochemical mechanisms that control the mobility of fluoride in a deep siliciclastic aquifer that is now targeted by a large-scale groundwater replenishment operation.

2. Materials and methods

2.1. Study site

The study site is located approximately 25 km north of the Perth metropolitan area, Western Australia (Fig. 1), where the feasibility of recycling wastewater through a combination of advanced water treatment (AWT) and MAR was comprehensively investigated over the last >15 years. The initial feasibility study phase included a detailed hydrogeological and geochemical characterisation campaign, and, most importantly, a groundwater replenishment trial (GWRT), during which 3.9 GL of highly purified recycled wastewater, sourced from the adjacent Beenyup wastewater treatment plant, was injected over a four-year period from 2010 to 2014 into the deep, siliciclastic Leederville aquifer. The interpretation of the site characterisation and the hydrochemical data collected during the GWRT (Higginson and Martin 2012) was supported by a suite of geochemical (Descourvieres et al., 2010a,b), solute/heat (Seibert et al., 2014) and reactive transport modelling studies (Seibert et al., 2016; Schafer et al., 2020). Based on the success of the GWRT, it was decided to pursue a staged implementation of large-scale groundwater replenishment (GWR). The first stage of the infrastructure construction was completed in 2017 and injection with a rate of 14GL/year has since commenced (Donn et al., 2017; Sun et al., 2020). Injection currently occurs through three wells (LRB1, LRB2 and LRB3) that are screened in the Leederville aquifer (max. injection rate 10-13 ML/day/bore) and an additional well (YRB1) that is screened in the deeper Yarragadee aquifer (Fig. 1). Similar to the GWRT, the source water for the full-scale GWR implementation is recycled wastewater, highly purified by three sequential treatment steps, i.e., ultra-filtration, reverse osmosis and UV disinfection (Higginson and Martin 2012; Moscovis 2013). The infrastructure for Stage 2 is currently under construction, which will shortly add another 14GL/year to the overall capacity. The additional capacity is provided by two wells screened in the Leederville aquifer (LRB4 and LRB5) and two additional wells (YRB2 and YRB3) screened in the Yarragadee aquifer (Fig. 1). The scheme forms now Australia's largest AWT-MAR operation.

2.2. Target aquifer and injectant characteristics

The target injection interval comprises the interbedded sand and shale lenses of the Wanneroo Member of the Cretaceous Leed-

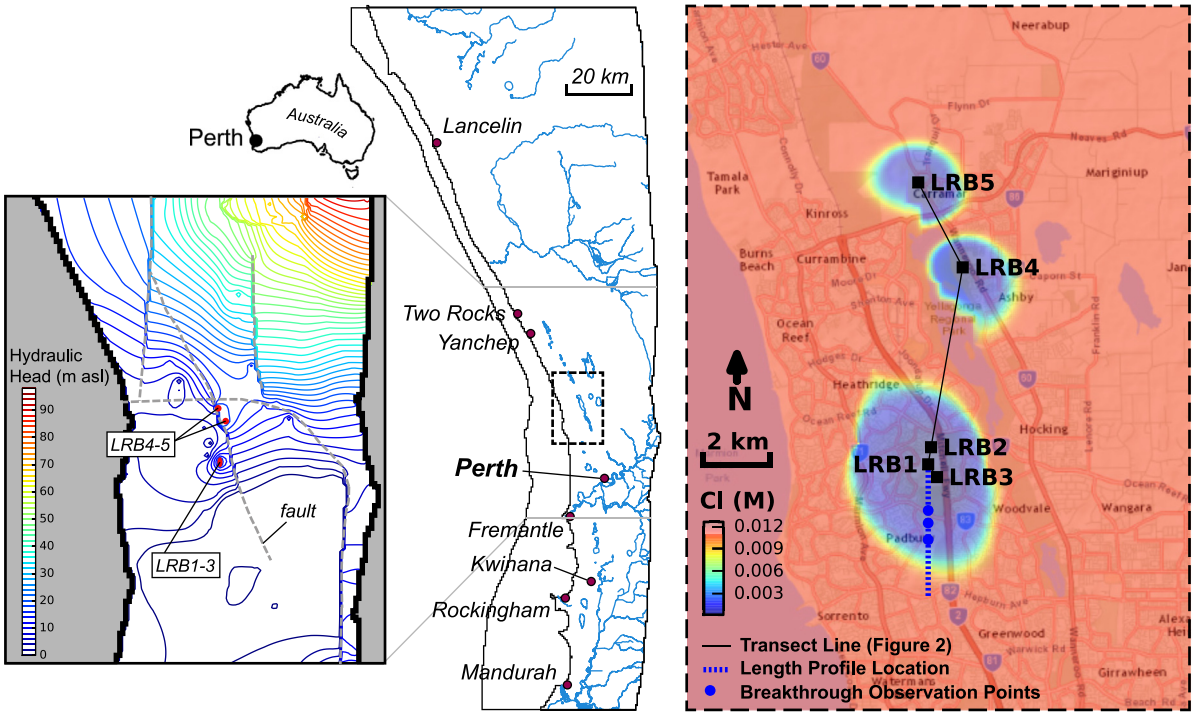

Fig. 1. Left: Simulated groundwater elevations (hydraulic heads) after 30 years simulation time. Centre: Location of the model domain representing the GWR-impacted section of the confined Leederville aquifer. The model domain extents over an area of 15 km × 21.5 km, comprising 344 column and 240 rows with a lateral grid discretisation of 62.5 m × 62.5 m. Right: Simulated chloride concentrations after 30 years simulation time, as indicated by the coloured shading.

Table 1
Average native groundwater and injectant compositions during the GWR.

Species	Unit	Native Groundwater (average of LMB1, LMB2 and LMB3)	Deionised Recycled Water (average injectant from Stage I)
pH	–	6.98 (sd = 0.24, n = 22)	7.03 (sd = 0.11, n = 53)
T emperature	°C	23.7 (sd = 1.47, n = 7)	26.8 (sd = 2.27, n = 35)
TDS	mg/L	589 (sd = 139, n = 21)	25.7 (sd = 7.88, n = 11)
Dissolved Oxygen	µM	–	518 (sd = 31.3, n = 78)*
Cl	µM	8081 (sd = 2084,n = 21)	190 (sd = 174,n = 11)
Na	µM	6497 (sd = 2142,n = 21)	334 (sd = 46.1,n = 11)
HCO3	µM	1172 (sd = 72.5,n = 21)	163 (sd = 24.3,n = 11)
Ca	µM	705 (sd = 70.8,n = 21)	below detection limit of 0.1 mg/L
Mg	µM	669 (sd = 228,n = 21)	below detection limit of 0.1 mg/L
Si	µM	430 (sd = 43,n = 21)	8.47 (sd = 2.29,n = 11)
K	µM	307 (sd = 50.1,n = 21)	22.6 (sd = 5.58,n = 11)
SO4	µM	233 (sd = 98.9,n = 21)	below detection limit of 0.1 mg/L
Fe (filtered)	µM	94.3 (sd = 32.7,n = 21)	below detection limit of 0.005 mg/L
N (total)	µM	15.6 (sd = 1.96,n = 14)	125 (sd = 28.1,n = 11)
Br	µM	10.1 (sd = 3.04,n = 21)	below detection limit of 0.02 mg/L
F	µM	5.34 (sd = 1.06,n = 21)	4.15 (sd = 1.45,n = 9)
FRP#	µM	1 measurement of 0.65 above detection limit of 0.01 mg/L (n = 11)	1 measurement of 0.32 above detection limit of 0.01 mg/L (n = 11)
P (total)	µM	3.33 (sd = 1.51,n = 14)	4 measurements above detection limit of 0.005 mg/L, range 0.32 - 1.03 (n = 11)
B	µM	2.44 (sd = 0.69,n = 14)	11.1 (sd = 2.27, n = 11)
Mn (filtered)	µM	1.07 (sd = 0.33,n = 21)	below detection limit of 0.001 mg/L
Al (filtered)	µM	0.23 (sd = 0.07,n = 13)	1 measurement of 0.26 above detection limit of 0.005 mg/L (n = 11)
I	µM	0.22 (sd = 0.03,n = 14)	below detection limit of (0.02 mg/L)

Note:.
* Measurements from field trial injection of recycled deionised water.
# FRP = Filterable Reactive Phosphorous (assumed to represent phosphate).

erville Formation (Leyland 2011; Timms et al., 2015), which is confined above and below by clayey units. The sediments of the Leederville Formation are a mature siliciclastic sequence that consists predominantly of quartz, kaolinite and K-feldspar, with trace coal fragments, pyrite, siderite, muscovite, biotite, chlorite, glauconite and CFA (Descourvieres et al., 2011; Schafer et al., 2018). The native groundwater (NGW) increases in salinity with depth over the injection interval from approximately 400 to 1100 mg/L (Table 1). Its hydrochemical composition varies from Na-Cl type groundwater near the top towards a Na-Cl-HCO_3 type groundwater at the base of the injection interval. In contrast, the highly purified wastewater is characterised by a very low ionic strength (TDS ~33 mg/L)

with particularly low divalent cation concentrations (~2.5 µM Ca^{2+}, ~5.0 µM Mg^{2+}) and a dissolved oxygen concentration of ~500 µM (Table 1).

2.3. GWR-induced groundwater flow and solute transport processes

The hydrogeological characterisation and the monitoring data collected during both the GWRT (Seibert et al., 2014) and GWR Stage 1 (Sun et al., 2020), suggest that, at the local scale, the injectant radially migrates away from the injection wells in strictly horizontal direction and preferentially in the sandy sections of the target aquifer, while flow and solute transport in the silty and clayey sections is negligible. The natural regional groundwater flow at the field site (hydraulic gradient ~0.0006), along with the potential impacts of seawater (the deeper aquifer systems exhibit relatively fresh water extending far offshore), are assumed negligible and therefore groundwater flow was controlled primarily by the MAR reinjection scheme. Over time, injectant transport is predicted to successively divert from the initially radial-symmetric pattern and to be increasingly influenced by the regional groundwater flow patterns and hydrogeological features such as faults and groundwater extraction wells that impact groundwater flow rates and directions (Fig. 1). The predictive model simulations performed by Sun et al. (2020) show that the injectant plume fronts migrate up to 4 km away from the respective injection locations in both the Leederville and the Yarragadee aquifer after 30 years of injection (Fig. 1). The model simulations also illustrate the clear hydraulic separation of the two GWR target aquifers that is imposed by the South Perth Shale.

2.4. Major GWR-induced geochemical changes and reactions

GWR results in significant groundwater quality changes in the Leederville aquifer. The majority of the observed changes can be attributed to the successive displacement of the native water by the injectant. However, the displacement of the native water causes a geochemical dis-equilibrium and therefore triggers a whole range of geochemical reactions. Underpinned by results from laboratory-scale incubation and column experiments (Descourvieres et al., 2010a,b), as well as detailed field observations (Higginson and Martin 2012), the model-based analysis of the GWRT demonstrated that pyrite oxidation was the primary geochemical reaction that was triggered by the injection. Pyrite oxidation is primarily triggered by the dissolved oxygen that is contained in the injectant (Prommer and Stuyfzand, 2005; Seibert et al., 2016):

$$FeS_2 + 3.75\,O_2 + 3.5\,H_2O \leftrightarrow Fe(OH)_3 + 2\,SO_4^{2-} + 4\,H^+ \quad (1)$$

and to some extent also by residual concentrations of nitrate that is also contained in the injectant:

$$FeS_2 + 3\,NO_3^- + 2\,H_2O \leftrightarrow Fe(OH)_3 + 2SO_4^{2-} + 1.5\,N_2 + H^+ \quad (2)$$

With pyrite oxidation being accompanied by the release of acidity, and the inherent buffering capacity of the injectant being low, proton exchange on sediment exchanger sites and the dissolution of trace minerals including aluminosilicates and siderite showed to be the main reactions to prevent a pH decline in the target aquifer and, potentially associated with it, an increase in metal(loid) mobility (Seibert et al., 2016; Sun et al., 2020).

2.5. Fluoride mobilisation

During the GWRT and GWR Stage 1, elevated fluoride (up to 58 μM) and phosphate concentrations (up to 55 μM) were observed at or near the injection plume front. Laboratory-based experimental work (Schafer et al., 2018) and the model-based interpretation of the GWRT (Schafer et al., 2020) identified that the source of both the fluoride and phosphate was the dissolution of CFA. The fluoride and phosphate breakthrough behaviour that was observed during the GWRT is considered to be a result of the incongruent dissolution of CFA where (i) a rapid proton exchange reaction primarily released fluoride and calcium, and (ii) a simultaneous equilibrium with a mineral-water interface layer of hydrated dibasic calcium phosphate (referred to as DCPsurface $\equiv CaHPO_4{\cdot}nH_2O$) released phosphate (Atlas and Pytkowicz 1977; Chaïrat et al., 2007a; Chaïrat et al., 2007b; Christoffersen et al., 1996; Gómez-Morales et al., 2013; Guidry and Mackenzie 2003; Tribble et al., 1995). Based on the analysed CFA composition, the two-step reaction could be represented by (Schafer et al., 2018; Schafer et al., 2020):

$$Ca_{9.75}Na_{0.25}(PO_4)_{5.37}(CO_3)_{0.55}F_{2.36}(OH)_{0.18} + 5.37H^+ + nH_2O \leftrightarrow\equiv Ca_{5.37}H_{5.37}(PO_4)_{5.37}\cdot nH_2O + 4.38Ca^{2+} + 0.25Na^+ + 0.55CO_3^{2-} + 2.36F^- + 0.18OH^- \quad (3)$$

$$\equiv Ca_{5.37}H_{5.37}(PO_4)_{5.37}\cdot nH_2O \leftrightarrow 5.37Ca^{2+} + 5.37HPO_4^{2-} + nH_2O \quad (4)$$

CFA dissolution and thus fluoride and phosphate release was found to occur because the divalent calcium contained in the injectant preferentially partitions onto cation exchanger sites, with the low aqueous calcium concentrations shifting the CFA equilibria that persisted with the NGW prior to GWR (Schafer et al., 2020).

3. Model-based assessment of AWT process modifications

3.1. Overview

Together with the induced spatially and temporally varying pH changes and other moving reaction fronts, the controls on fluoride mobility are complex and highly nonlinear, suggesting that any systematic exploration of the feasibility of successful and appropriately dosed AWT process modifications is best achieved through a process-based numerical modelling approach. We therefore use predictive reactive transport modelling as a tool to assess and compare the efficiency of a suite of potential AWT process modifications. The simulations rely on our previously developed and comprehensively calibrated and evaluated reactive transport modelling framework (Sun et al., 2020), which includes a process-based simulation of the fluoride release and attenuation mechanisms. The modelling framework relies on the conceptual hydrogeochemical model that fluoride mobilisation occurred as a result of CFA dissolution at locations where the arrival of the GWR-induced injectant plume changed the persisting geochemical equilibrium between the NGW and the aquifer sediments. The model-based interpretation of fluoride mobility during the GWRT illustrated the complex interactions that occur as a result of (i) the low ionic strength of the injectant and (ii) the critical role that cation exchange can play on decreasing aqueous calcium concentrations and therefore inducing CFA dissolution (Schafer et al., 2020). In the following we only provide a brief summary of the employed numerical model framework, while the full details of the large-scale flow, solute and reactive transport simulations are provided in Sun et al. (2020). Additional details of the conceptual/numerical model aspects concerning fluoride mobility can be found in Schafer et al. (2018) and Schafer et al. (2020). In this study, our model-based assessment is focused on the Leederville aquifer. However, our results will also be largely transferrable to the deeper Yarragadee aquifer and, more broadly, to many other sites of similar geochemical characteristics that are subjected to AWT-MAR.

3.2. Numerical model framework

3.2.1. Groundwater flow and solute transport

The site-specific groundwater flow and solute transport behaviour at this AWT-MAR study site has been intensively characterised at the local, GWRT scale, supported by a wide range of geophysical logging and other techniques (Higginson and Martin 2012). At the GWRT scale, the constructed numerical flow and solute transport models were set up at a high vertical resolution to capture the strong vertical heterogeneity of the Leederville aquifer (Seibert et al., 2014). Each of the considered model layers was assumed to be hydrogeologically and geochemically homogeneous in the lateral direction. Over the GWRT scale, this assumption was deemed to be reasonable, supported by the solute transport modelling results that showed a good agreement with GWRT observations. However, for the simulations assessing the long-term and larger-scale solute and reactive transport behaviour the assumption that the layering assumed in the local-scale models would be continuous fails to hold. To overcome this limitation, Sun et al. (2020) recently developed a pragmatic upscaling approach that allowed to perform computationally efficient large-scale predictions of the GWR-induced flow, solute and reactive transport behaviour. The upscaling process involved lumping the heterogenous solute transport behaviour into a vertically integrated surrogate model. The key transport characteristics, which are affected by a high fraction of silty/clayey aquifer sections were successfully captured by invoking a dual domain mass transfer model (DDMT) (Feehley et al., 2000; Schweizer et al., 2018; Underwood et al., 2018), which conceptually separates the model domain into a mobile and an immobile fraction, with the former fraction capturing the preferential transport in the Leederville aquifer's sandy layers and the latter fraction representing the silty/clayey layers that make a negligible contribution to the aquifer's transmissivity and to the mass fluxes away from the injection wells. The large-scale groundwater flow behaviour is captured by downscaling the simulation results of the Perth Regional Aquifer Modelling System (PRAMS) (CyMod_Systems 2009, 2014; Davidson and Yu 2008; Siade et al., 2020; Siade et al., 2017) to the subdomain that was selected for the assessment of the large-scale GWR impacts. Further details of the model construction and the up- and down-scaling procedures are provided in Sun et al. (2020). Fig. 1 illustrates the location of the model subdomain, simulated groundwater head contours for the considered 28GL/year GWR scheme and the simulated evolution of the injectant transport over a 30-year period.

3.2.2. Reaction transport model framework

Based on the insights gained from the GWRT-scale flow and conservative transport simulations, long-term, large-scale reactive transport simulations were performed by Sun et al. (2020) to assess the two potentially most critical groundwater quality changes that could result from GWR. These two critical issues were (i) to develop a quantitative estimate of the longevity of the previously identified pH buffering mechanism, thus minimising the risk of metal mobilisation and (ii) to understand the long-term large-scale mobility of fluoride, specifically on whether there could be any accumulative "snow plough" effects (Starr and Parlange 1979) at the injection plume front that could lead to successively increasing fluoride concentrations at increasing distance from the injection wells. To simulate the key reactions impacting the fate of fluoride, incongruent CFA dissolution (Reaction 3) was incorporated as an equilibrium exchange reaction, and the DCPsurface (Reaction 4) was considered as an equilibrium mineral reaction. The associated equilibrium constants and some other important reaction parameters are provided in Table 2. Further details of the developed reaction network, its implementation into the reaction database and its evaluation against a wide range of field data are discussed in Seibert et al. (2016), Schafer et al. (2018) and Sun et al. (2020). The model simulation results obtained by Sun et al. (2020) suggested that the maximum fluoride concentrations would not rise above the levels that were already observed at the local scale during the GWR. For the present assessment of potential AWT process modifications that could minimise fluoride mobilization, these model simulations were used as the base case against which the efficiency of any injectant modification was benchmarked.

3.3. Investigated injectant modifications

A total of five different options for modifying the injectant composition were tested to evaluate whether they were effective in minimising the release of fluoride during long-term large-scale GWR into the Leederville Formation (Table 3). The selected scenarios either involve (i) a direct increase of calcium concentrations through the amendment of calcium-bearing chemicals during AWT, (ii) an indirect increase of aqueous calcium concentrations by promoting cation exchange or (iii) injectant treatment that is aimed at causing a pH increase within the targeted aquifer zones as a way to suppress fluoride release (Eq. (3)). Each of the five amendment variants is described in more detail below and the corresponding (hypothetical) injectant water compositions for the different model variants are listed in Table 3. The investigated amendments were tested for different amendment doses, from those that caused only minor reduction in fluoride, to those that almost completely prevented fluoride concentrations to rise above background levels.

3.3.1. Calcium chloride

The effectiveness of amending the injectant with calcium chloride ($CaCl_2$) was explored by model variants V1.1 – V1.5. $CaCl_2$ was selected because it has the benefit of directly adding calcium ions to the injectant and therefore to potentially suppress CFA dissolution. The potential for $CaCl_2$ to be effective is underpinned by earlier experimental work by Borgnino et al. (2013) that showed that the addition of calcium successfully inhibited fluorapatite dissolution at circumneutral pH. Five different calcium amendment doses, i.e., 1×10^{-4} M, 5×10^{-4} M, 5×10^{-3} M, 3×10^{-3} M and 5×10^{-3} M $CaCl_2$ were tested in model variants V1.1–1.5, respectively.

3.3.2. Calcium hydroxide

The model variants V2.1 and V2.2 involved the amendment of calcium hydroxide ($Ca(OH)_2$). It has the potential benefit of directly adding calcium ions while also elevating the injectant pH, both of which would be expected to suppress CFA dissolution. $Ca(OH)_2$ is currently being applied as an amendment for the MAR of low ionic strength water in Orange County, California, where it is mainly applied to limit the potential corrosion of concrete pipes (Fakhreddine et al., 2015). Two different calcium hydroxide amendment doses, i.e., 1×10^{-4} M and 3×10^{-4} M were tested in model variants V2.1 and V2.2, respectively. Note, that the amount of $Ca(OH)_2$ that can be added is limited by the potential for calcite precipitation (Fakhreddine et al., 2015), which is estimated to occur at a concentration of ~3×10^{-4} M $Ca(OH)_2$ under atmospheric carbon dioxide partial pressure.

3.3.3. Sodium chloride

The model variants V3.1 – V3.5 involved the addition of NaCl. Addition of sodium was expected to displace calcium ions from sediment exchanger sites causing an increase in aqueous calcium concentrations and thus suppress CFA dissolution. Five doses, i.e., 1×10^{-4} M, 5×10^{-4} M, 5×10^{-3} M, 3×10^{-3} M and 5×10^{-3} M NaCl were trialled in model variants V3.1 – V3.5.

Table 2
Reaction network.

Mineral reactions		equilibrium/kinetic^	log $K_{SP}^{25°C}$
$Fe(OH)_3$ (amorphous)	$Fe(OH)_3(a) + 3H^+ \leftrightarrow Fe^{3+} + 3H_2O$	equilibrium	4.89[1]
Glauconite	$Ca_{0.02}K_{0.85}Fe^{III}_{0.03}Mg_{1.01}Fe^{II}_{0.05}Al_{0.32}Si_{3.735}O_{10}(OH)_2 + 7.07H^+ + 7H_2O \leftrightarrow 0.02Ca^{2+} + 0.85K^+ + 1.03Fe^{3+} + 1.01Mg^{2+} + 0.05Fe^{2+} + 0.32Al^{3+} + 3.735H_4SiO_4 + 4.53H_2O$	kinetic*	8.03[2]
Pyrite	$FeS_2 + 2H^+ + 2e^- \leftrightarrow Fe^{2+} + 2HS^-$	kinetic*	−18.48[1]
Siderite	$FeCO_3 \leftrightarrow Fe^{2+} + CO_3^{2-}$	kinetic*	−10.89[1]
Ferrous iron oxidation	$Fe^{2+} + 0.25O_2 + H^+ \leftrightarrow Fe^{3+} + H_2O$ $Fe^{2+} + 0.2NO_3^- + 1.2H^+ \leftrightarrow Fe^{3+} + 0.1N_2 + 0.6H_2O$	kinetic*	na
Sediment organic matter oxidation	$CH_2O + O_2 \leftrightarrow HCO_3^- + H^+$ $CH_2O + 0.8NO_3^- + 0.8H^+ \leftrightarrow HCO_3^- + 0.4N_2 + H^+ + 0.4H_2O$	kinetic*	na
Cation exchange half reactions#		**$logK_{SC}^{25°C}$**	
$Na^+ + X^- \leftrightarrow NaX$		0[1]	
$Ca^{2+} + 2X^- \leftrightarrow CaX_2$		0.8[1]	
$Mg^{2+} + 2X^- \leftrightarrow MgX_2$		0.6[1]	
$K^+ + X^- \leftrightarrow KX$		0.7[1]	
$H^+ + X^- \leftrightarrow HX$		5.08[3]	
$Fe^{2+} + 2X^- \leftrightarrow FeX_2$		0.44[1]	
$Mn^{2+} + 2X^- \leftrightarrow MnX_2$		0.52[1]	
$Sr^{2+} + 2X^- \leftrightarrow SrX_2$		0.91[1]	
$Ba^{2+} + 2X^- \leftrightarrow BaX_2$		0.91[1]	
$Al^{3+} + 3X^- \leftrightarrow AlX_3$		0.41[1]	
$AlOH^{2+} + 2X^- \leftrightarrow AlOHX_2$		0.89[1]	
Equilibrium with DCPsurface on CFA		**$logK_{SP}^{25°C}$**	
DCPsurface	$CaH(PO)_4.H_2O \leftrightarrow Ca^{2+} + H(PO)_4^{2-} + H_2O$	−10.07[4]	
CFA proton exchange#		**$logK_{SC}^{25°C}$**	
CFA proton exchange	$\equiv CfCa_{4.38}Na_{0.25}(CO_3)_{0.55}F_{2.36}(OH)_{0.18} + 5.37H^+ \leftrightarrow 4.38Ca^{2+} + 0.25Na^+ + 0.55CO_3^{-2} + 2.36F^- + \equiv CfH_{5.37}$ (where ≡Cf represents surface ≡CaPO4 groups on CFA)	0.59[4]	

Note:.
* refer to Seibert et al. (2016) for full details of the employed kinetic rate expressions;.
# selectivity coefficients for exchange reactions have been defined using the Gaines and Thomas equivalent fractions convention (Appelo and Postma 2005).
[1] (Parkhurst 2015).
[2] (Pham et al., 2011).
[3] (Seibert et al., 2016).
[4] (Chaïrat et al., 2007a; Schafer et al., 2018).

Table 3
Model scenario variants of different amendments applied to the injectant water and concentrations of selected species.

Scenario	Variants	Added amendment concentration	DO µM	Na µM	K µM	Mg µM	Ca µM	Cl µM	HCO3 µM	SO4 µM	pH
V0 base case	–	–	500	334	23	0	0	166	164	0	7.035
V1 $CaCl_2$	V1.1	0.0001M	500	334	23	0	100	366	164	0	7.035
	V1.2	0.0005 M	500	334	23	0	500	1166	164	0	7.035
	V1.3	0.001 M	500	334	23	0	1000	2166	164	0	7.035
	V1.4	0.003 M	500	334	23	0	3000	6166	164	0	7.035
	V1.5	0.005M	500	334	23	0	5000	10,166	164	0	7.035
V2 $Ca(OH)_2$	V2.1	0.0001 M	500	334	23	0	100	134	345	0	7.707
	V2.2	0.0003 M	500	334	23	0	300	134	739	0	8.040
V3 NaCl	V3.1	0.0001 M	500	434	23	0	0	266	164	0	7.035
	V3.2	0.0005 M	500	834	23	0	0	666	164	0	7.035
	V3.3	0.001 M	500	1334	23	0	0	1166	164	0	7.035
	V3.4	0.003 M	500	3334	23	0	0	3166	164	0	7.035
	V3.5	0.005 M	500	5334	23	0	0	5166	164	0	7.035
V4 synthetic sea salt	V4.1	0.0001 M	500	420	24	10	2	266	164	5	7.035
	V4.2	0.0005 M	500	463	32	48	9	666	165	26	7.035
	V4.3	0.001 M	500	1191	41	97	19	1166	167	52	7.035
	V4.4	0.003 M	500	2906	79	290	56	3166	174	155	7.035
	V4.5	0.005 M	500	4620	116	483	94	5166	180	258	7.035
V5 de-oxygenation	–	–	0	334	23	0	0	166	164	0	7.035

3.3.4. Synthetic sea salt

The amendment of synthetic sea salt was explored as it has the benefit of (i) the direct addition of calcium ions into the injectant and (ii) adding sodium, which can displace calcium from sediment exchanger sites or prevent the partitioning of aqueous calcium onto the exchanger sites. The tested synthetic sea salt concentrations were 1×10^{-4} M, 5×10^{-4} M, 5×10^{-3} M, 3×10^{-3} M and 5×10^{-3} M chloride for V4.1 – V4.5, respectively, where the stoichiometric ratio of the major ions (chloride, sodium, bicarbonate, magnesium, sulphate, potassium, calcium) and fluoride that occurs in standard seawater (DOE 1997) was applied to the (current) base injectant composition (Table 3). Note that seawater has been found to be in equilibrium with the surface of CFA (Atlas and Pytkowicz 1977; Atlas 1975).

3.3.5. Deoxygenation

The final model variant V5 involved the hypothetical complete deoxygenation of the injectant. This model variant was included to test whether the reduction of the electron acceptor capacity with the injectant (nitrate would still be present) could minimise the release of acidity sufficiently to have indirect benefits on reducing the level of fluoride mobilisation.

4. Results and discussion

4.1. Simulated long-term geochemical response to gwr and associated fluoride behaviour

The large-scale reactive transport simulation for the base case V0 illustrates the anticipated long-term behaviour of fluoride in the Leederville aquifer for a 28 GL/year GWR scheme. Fig. 2 shows 2D contour plots of groundwater fluoride concentrations after 5, 10 and 30 years, as well as the corresponding concentrations of calcium and the groundwater pH, while Fig. 3 shows simulated breakthrough curves at selected locations at increasing radial distances from injection well LRB1. As can be seen in Fig. 2, the injection plumes initially grow radially but the shapes of the injection plumes are successively changing as the influence of the background groundwater flow increases and the influence of the GWR-induced flow decreases with increasing distance from the various injection well locations. The simulations show the development of four distinct geochemical zones along the radial direction, which evolve as the injectant plumes grow. These four zones (Z1-Z4) numbered from the injection front towards the injection well (right to left) are marked in the concentration length profiles in Fig. 4 by different shadings. The zonation identified in this study is largely consistent with the zonation that was found to evolve during the GWRT, which was discussed in more detail by Schafer et al. (2020). Understanding the key mechanisms that underly the formation of these zones is critical for deciphering the variations in the response to the tested modifications in the hydrochemical composition of the injectant. Therefore, salient features of the evolution of geochemical zones for the base case are discussed below.

The first zone, Z1, marks the mixing zone at the injectant plume front. In this zone chloride concentrations drop sharply from the elevated NGW concentrations towards the much lower chloride concentrations of the injectant (Fig. 4a-c). Despite its chemically inert behaviour, at larger radial distances the simulated chloride concentrations do not decline completely to the level of the injectant concentrations. This is explained by the chloride enrichment that occurs through the simulated kinetically controlled physical DDMT process, which is driven by the chloride concentration gradient between the mobile domain and immobile domains. The DDMT process represents the more gradual displacement of NGW from the Leederville aquifer's low-permeability zones (immobile domain) compared to that of the sandy permeable layers (mobile domain) by the low ionic strength injectant. Due to the kinetic control of the DDMT process and the groundwater flow velocities that decrease with increasing distance from injection wells, the impact of the DDMT gradually becomes more pronounced at larger (radial) distances, which results in increased tapering of chloride at the injection front (Fig. 4a-c). Within Z1, calcium concentrations also abruptly decrease with distance from LRB1, which disturb the CFA equilibrium condition, thereby inducing a rise in groundwater fluoride concentrations. The fluoride concentrations within Z1 increase from their NGW concentrations levels towards their maximum concentrations at the Z1/Z2 interface (Fig. 4d-f). Within Z1 the pH rises to ~7.3 during the early years of GWR as a result of proton exchange with Ca (Fig. 4j-l) and thus above the pH within both the injectant and the NGW.

The adjacent zone, Z2, is characterized by the peaking fluoride concentrations at the interface with Z1 which then decrease within Z2 towards Z3 (Fig. 4d-f). In this zone the much lower ionic strength of the injectant results in a higher proportion of calcium on exchanger sites compared to that occurring in Z1 and in the native aquifer (Fig. 4y-aa). As the calcium concentration in the injectant is below detection (Tables 2 and 3), calcium in this zone is derived from DDMT and, more importantly, from the dissolution of CFA, which decreases towards the injection front (insets Fig. 4v-x). Calcium on the cation exchanger sites (X) therefore increases within this zone towards the injection well (insets Fig. 4m-o), exchanging for both sodium (insets in Fig. 4p-r) and protons (insets in Fig. 4s-u). At later times, when the injectant plume has become much larger, the proportion of calcium derived via mass transfer from low permeability layers dominates over the calcium derived from CFA dissolution (Fig. 4g-i). DDMT also affects all other groundwater constituents in that it causes a successive mixing of the injectant with NGW at the injection front causing the concentrations of all species to more gradually increase towards NGW concentrations.

Zone Z3 is characterized by significant calcium removal from the groundwater due to greater cation exchange (Fig. 4g-i, m-o). Accordingly, the fraction of calcium occupying the cation exchanger sites (CaX_2) is increased in this zone (Fig. 4m-o, y-aa), while sodium (Fig. 4p-r) and proton concentrations (Fig. 4s-u) on the exchanger site (NaX and HX) are lower. In this zone pH is also elevated compared to the pH of the injectant (Table 3) as well as the NGW (Fig. 4j-l). The ratio of hydrogen activity to calcium activity is lower in this zone compared to the adjacent Z2 (red shading) (Fig. 4ab-ad) and fluoride concentrations are relatively low and significantly below NGW concentrations.

The geochemical zone Z4 resides in the vicinity of the injection well and is the only zone where pyrite oxidation occurs as all oxidants are exhausted at larger travel distances. This zone is characterized by a lower pH relative to the pH of the injectant (Fig. 4j-l) and high calcium concentrations considering the deionized injectant started with negligible calcium (Tables 2 and 3) (note calcium concentrations are plotted on a logarithmic scale). In this zone protons generated from pyrite oxidation displace calcium (Fig. 4m-o) and sodium (Fig. 4p-r) from the cation exchanger and dissolve CFA (Eq. (3)) (Fig. 4v-x). Consequently, fluoride concentrations are low in this zone (Fig. 4d-f) and are similar to the concentrations in the deionized injectant of 4 µM (Table 3)

4.2. Performance and mechanisms controlling amendment efficacy for fluoride attenuation

4.2.1. Performance of different amendments

The reactive transport model was used to assess whether CFA dissolution could be suppressed through the modification of the injectant composition. All the simulated scenarios for injectant modifications, except for the deoxygenation scenario V5, were found to reduce maximum fluoride concentrations compared to the base case V0, as shown by selected breakthrough curves for radially increasing distances from the injection location LRB1 (Fig. 3). The efficacy of the different amendments in reducing maximum fluoride concentrations for varying dosages is summarized in Fig. 5. It can be seen, that for the lowest dose (1×10^{-4} M) all amendment types had negligible impact on reducing maximum fluoride concentrations relative to the base case (V0). However, the maximum fluoride concentrations decreased consistently for all amendment types with increasing dosage. The release of fluoride can be almost entirely suppressed once dosages reach and exceed concentrations of 1×10^{-3} M $CaCl_2$, NaCl or sea salt.

Amendment of the injectant with $CaCl_2$ (V1.1–1.5) produced the greatest reduction of maximum fluoride concentrations at all

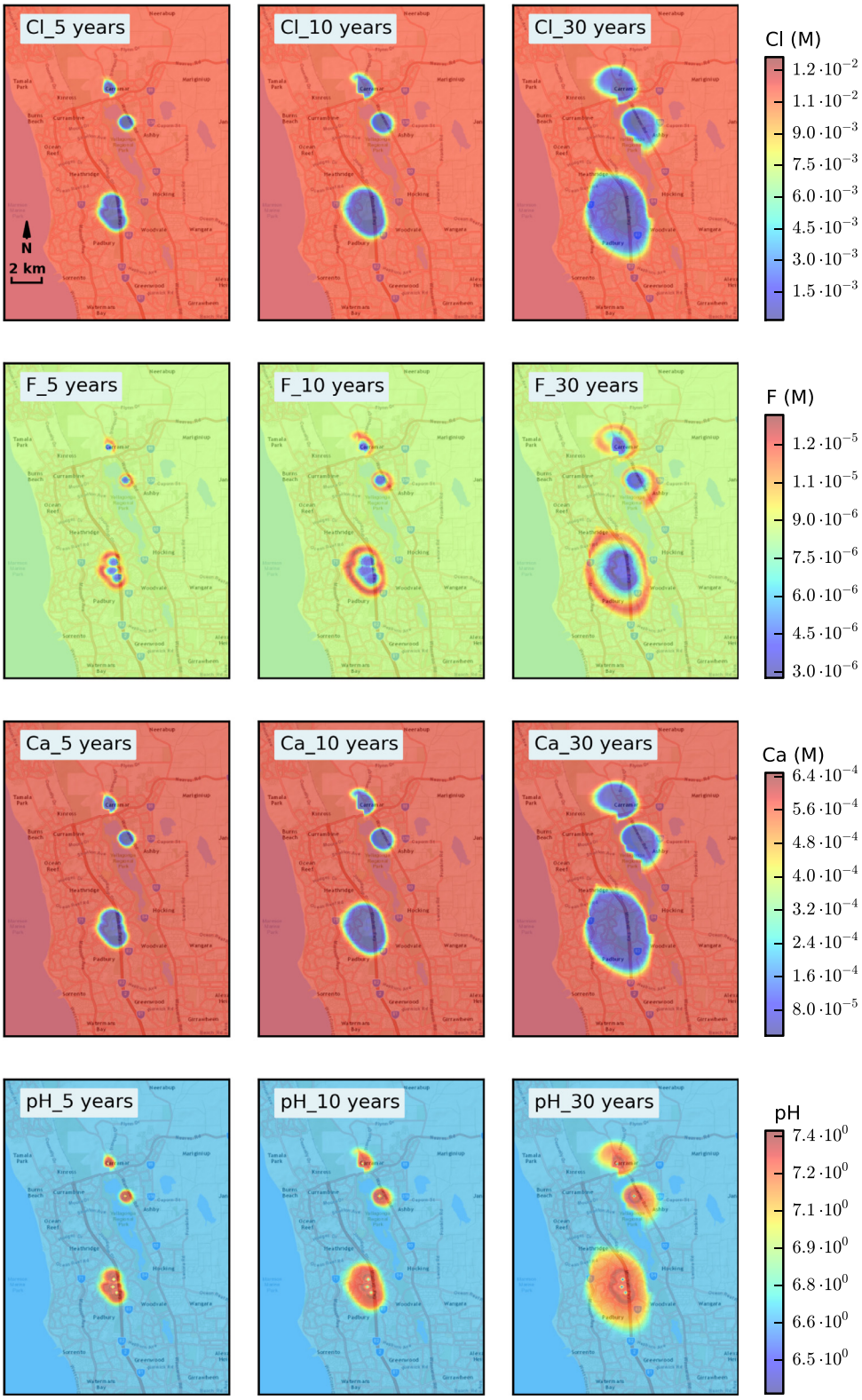

Fig. 2. Simulated fluoride, calcium and chloride concentrations, and pH in the Leederville aquifer after 5, 10 and 30 years for the base case (V0).

dosages except for 1×10^{-3} M, where NaCl (V3.3) and sea salt (V4.3) perform slightly better (Fig. 5). Unsurprisingly, the performance of sea salt (V4.1–4.5) and NaCl (V3.1–3.5) are similar, with sea salt consistently producing slightly lower maximum fluoride concentrations for the investigated range of dosages. The amendment of $Ca(OH)_2$ (V2.1–2.2) performs similarly to NaCl and sea salt. However, as discussed above, the application of $Ca(OH)_2$ is limited by the solubility of calcite, precluding the application of sufficiently high dosages. With the maximum applicable dosage of $Ca(OH)_2$ (3×10^{-4} M; V2.2) only a relatively modest reduction in the maximum fluoride concentration is achieved (Fig. 5).

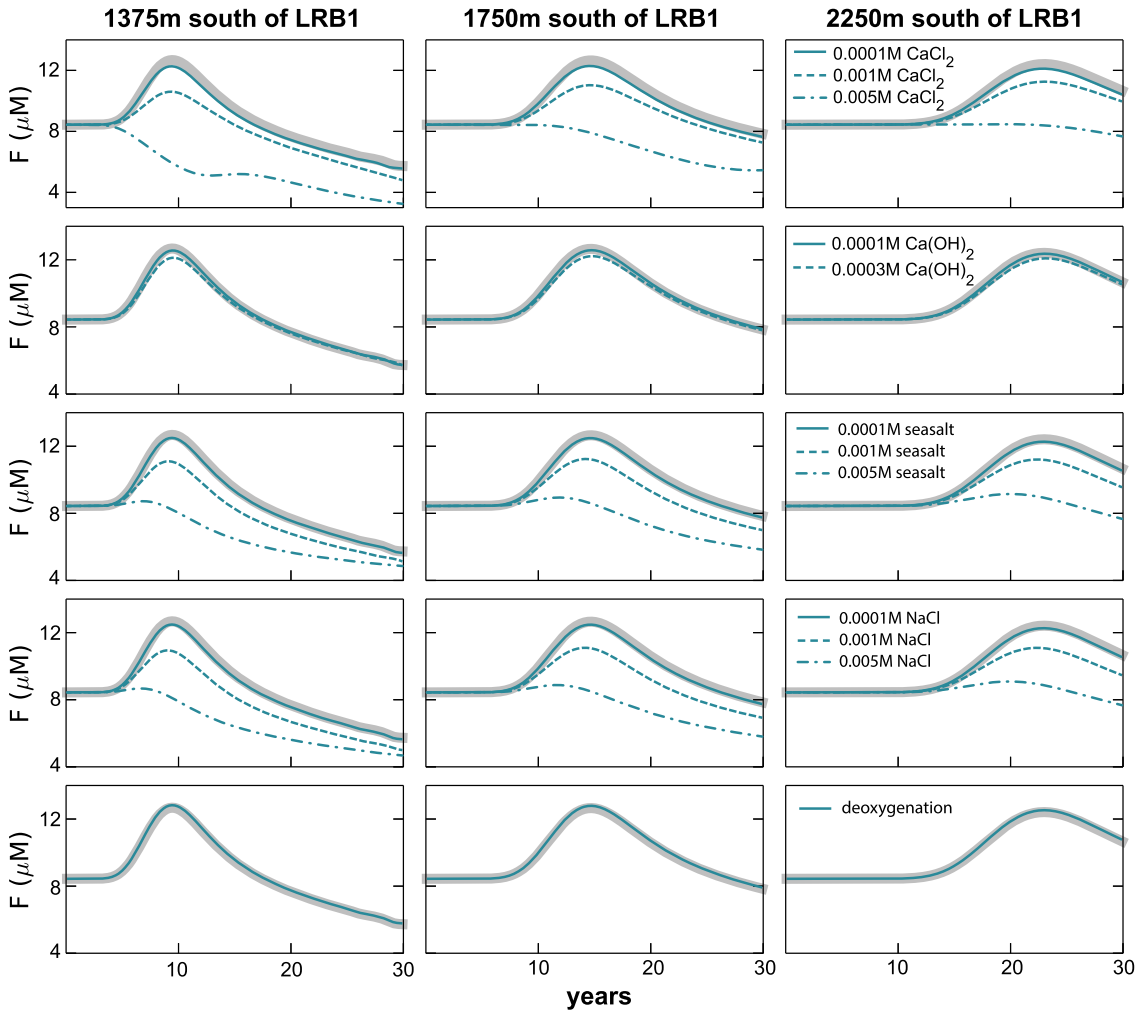

Fig. 3. Breakthrough curves for fluoride at 1375 m, 1750 m and 2250 m distance south of the injection well LRB1 (Fig. 1) for different pre-treatment amendments at selected dosages. The base case (V0) is shown by the thick pale grey line on each plot for comparison.

4.2.2. Geochemical mechanisms controlling amendment efficacy for fluoride attenuation

The aqueous calcium concentration was a major control for regulating CFA solubility. To illustrate the role of calcium, two of the investigated variants, both of similar dosing, i.e., 1×10^{-3} M $CaCl_2$ (V1.3) and 1×10^{-3} M NaCl (V3.3) are compared with the base case (V0) in Fig. 4. Both variants V1.3 and V3.3 develop a similar geochemical zonation pattern to V0. However, throughout the different geochemical zones, both V1.3 and V3.3 maintain consistently higher groundwater calcium concentrations than V0 (Fig. 4g-i), either due to direct addition (V1.3) or due to sodium displacing calcium from sediment exchanger sites. In either case the higher calcium concentration decreases CFA solubility and consequently suppresses fluoride release (Eq. (3)).

Despite calcium playing a central role in controlling fluoride release, the direct addition of $CaCl_2$ does not necessarily yield the best long-term results for all dosages considered. Variant V3.3 with NaCl performed marginally better than V1.3 with $CaCl_2$ after 30 years. This is due to a greater reduction in pH in V1.3, which induces some additional CFA dissolution and consequently fluoride release. The lower pH is the result of higher calcium concentrations in V1.3 displacing more hydrogen from sediment exchanger sites. The effect of reduced pH in Z3 for V1.3 is not significant at higher dosages (e.g., V1.4 and 1.5) (Fig. 6j-l). From the result of V1.4 it can be seen that due to the much higher calcium concentrations in the injectant, the proportion of calcium on exchanger (CaX_2) sites decreases significantly to well below that occurring under NGW conditions (Fig. 6j-l). As the proportion of calcium attenuated on exchanger sites decreases, higher calcium concentrations were able to propagate closer to the injection front, where they more effectively suppress CFA dissolution (Fig. 6d-f, m-o).

As mentioned before, the performance of the sea salt amendments (V4.1–4.5) were similar to the NaCl amendments (V3.1–3.5) (Fig. 5). This similarity results from the sodium concentrations for each of the corresponding variants being similar, thus causing an equivalent extent of competitive exchange with calcium on sediment exchange sites. However, the sea salt amendments (V4.1–4.5) consistently produced slightly lower maximum fluoride compared to NaCl (V3.1–3.5) amendments, demonstrating that the relatively small amount of additional calcium in the sea salt amendments (Table 3) has an appreciable effect.

The pH is also a strong control that regulates the release and attenuation of fluoride. Nevertheless, the variants designed to increase that pH, either by addition of $Ca(OH)_2$ (V2.1-V2.2) or minimising pyrite oxidation via deoxygenation (V5), were found to be less efficient at reducing fluoride concentrations (Fig. 7). Despite the injectant pH for V2.1 and V2.2 being elevated to 7.71 and 8.04, respectively, the substantial pH buffering effect of the sediment's cation exchanger site (X) prevented any significant rise of the pH (Fig. 7d-e). As calcium displaced protons on the exchanger sites

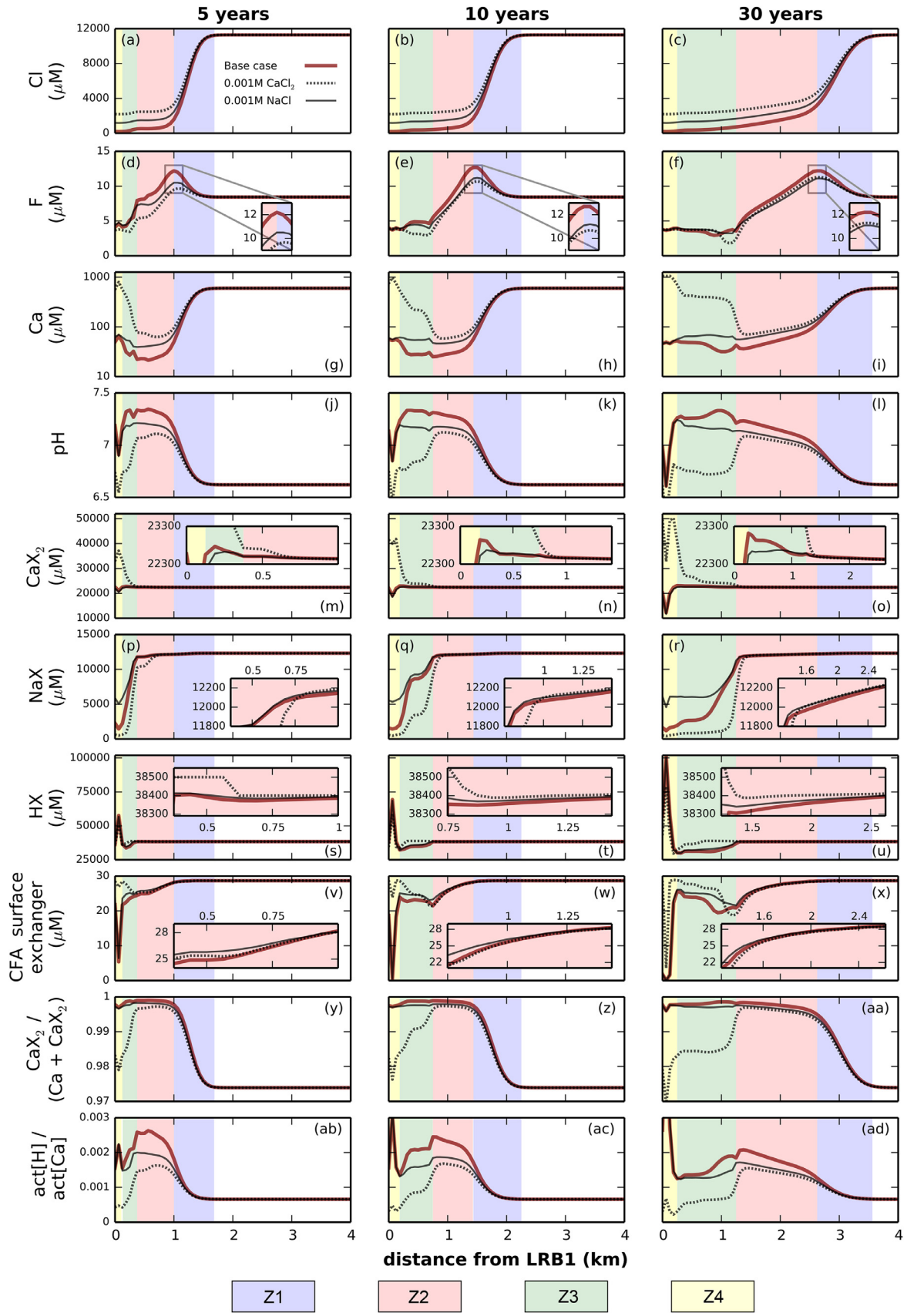

Fig. 4. Concentration profiles in radial direction from LRB1 (see Fig. 1 for location of profiles) showing key species and ratios after 5, 10 and 30 years. Results for the base case (V0) are indicated by thick maroon lines, results for amendment of 0.001 M $CaCl_2$ (V1.3) are shown by black dotted lines) and thin black lines indicate the results for amending 0.001 M NaCl (V3.3).

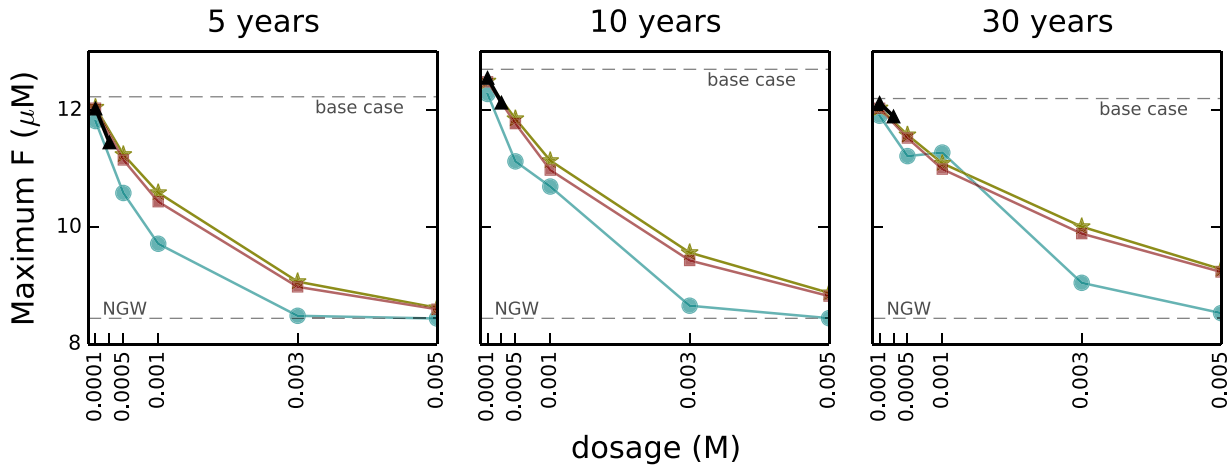

Fig. 5. Maximum fluoride concentration along the length profile line (Fig. 1) after 5, 10, and 30 years simulation time as a function of amendment dosage. $CaCl_2$ – blue circles; sea salt – maroon squares; NaCl – dark yellow stars; $Ca(OH)_2$ – black triangles.

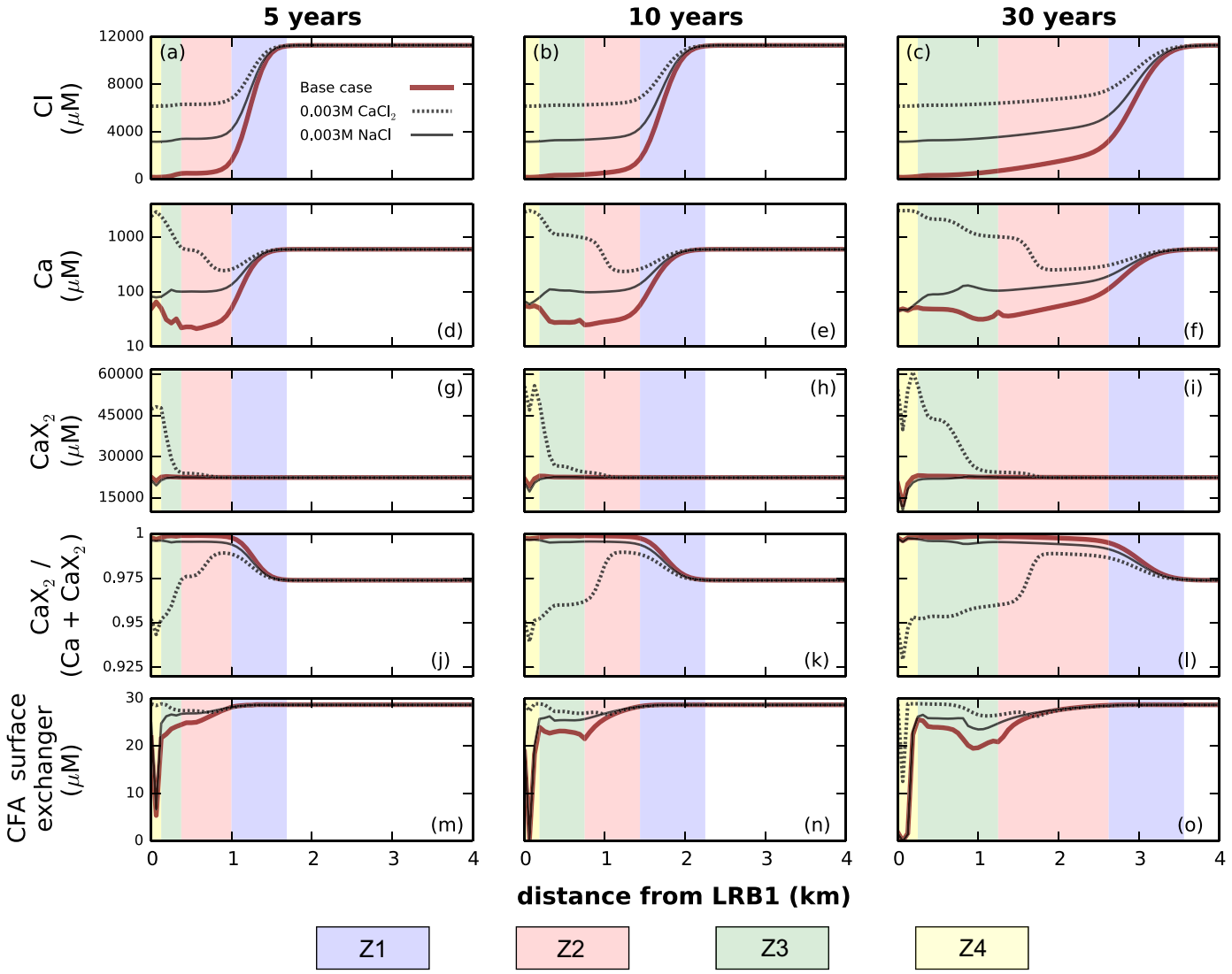

Fig. 6. Concentration profiles in radial direction from LRB1 (see Fig. 1 for location of profiles) showing key species and ratios after 5, 10 and 30 years. Results for the base case (V0) are indicated by thick maroon lines, results for amendment of 0.003 M $CaCl_2$ (V1.4) are shown by black dotted lines) and thin black lines indicate the results for amending 0.001 M NaCl (V3.4).

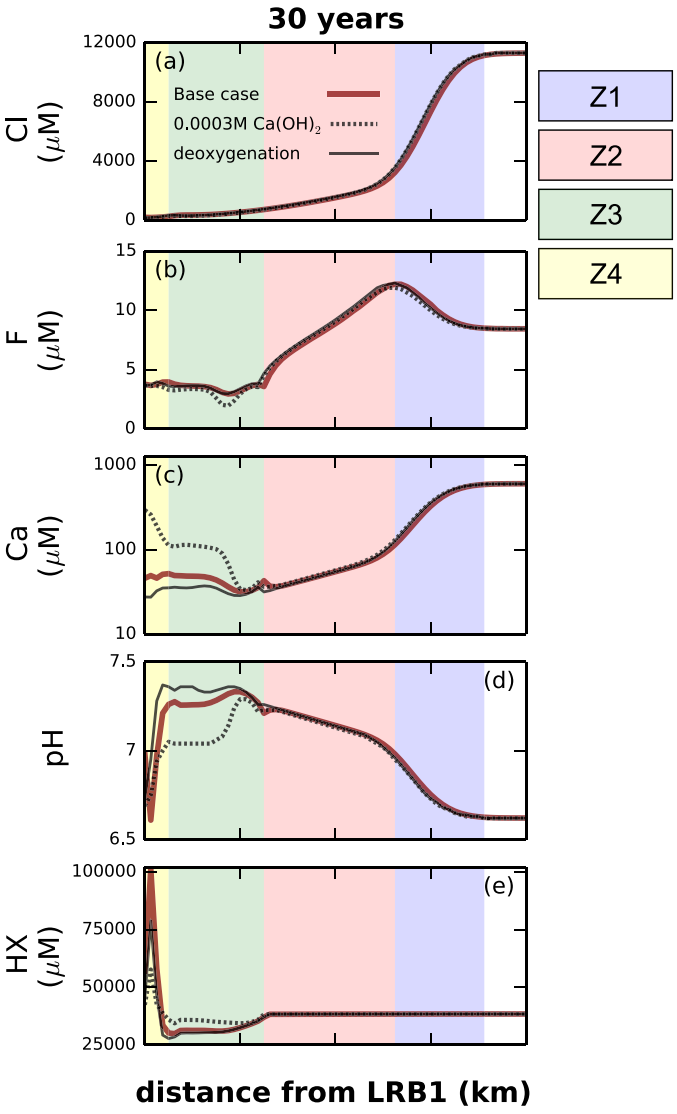

Fig. 7. Concentration profiles in radial direction from LRB1 (see Fig. 1 for location of profiles) showing key species after 5, 10 and 30 years. Results for the base case (V0) are indicated by thick maroon lines, results for amendment of 0.0003 M $Ca(OH)_2$ (V2.2) are shown by black dotted lines) and thin black lines indicate the results for deoxygenation (V5).

these model variants (V2.1-V2.2) produced similar calcium concentration profiles and consequently the release of fluoride was similar to the base case. The small reduction in fluoride by the 3×10^{-4} M $Ca(OH)_2$ (V2.2) amendment (Figs. 6 and 7b) is primarily due to the increased calcium concentration rather than changes to groundwater pH.

4.2.3. Additional operational considerations

Significant reductions of fluoride released from CFA due to the injection of low ionic strength water amended with $CaCl_2$, NaCl or sea salt can be achieved at moderate dosages of 1×10^{-3} M. While the greatest reductions of fluoride generally occurred for the $CaCl_2$ amendments (V1.1–1.5) the declining performance of the 1×10^{-3} M $CaCl_2$ (V1.3) dosage with time may preclude $CaCl_2$ being considered the best option at moderate dosages (Fig. 5). As a small amount of fluoride is considered beneficial for health (Sazakli et al., 2007; WHO 2017), complete suppression of fluoride release during MAR is not desired. Consequently, dosage of injectant with NaCl or sea salt at 1×10^{-3} M would achieve the best cost-effective approach for a 30–40% reduction of maximum fluoride (Fig. 5). While costs of implementing the sea salt and NaCl amendments are expected to be similar, the amendment of sea salt has the additional advantage of adding magnesium, which is considered a health benefit (Birnhack et al., 2011), as well as sulphate, which increases corrosion protection from metal pipes (Tang et al., 2006a; Tang et al., 2006b).

5. Conclusions

Reactive transport modelling was used to assess different pre-treatment amendments for highly purified recycled wastewater with respect to their effectiveness at reducing fluoride mobility during large-scale groundwater replenishment. The model results indicate that amendments that increase dissolved calcium concentrations either by direct addition of calcium-bearing chemicals or by manipulating sediment exchange reactions are effective at reducing CFA dissolution and therefore fluoride release. On the other hand, pre-treatment strategies attempting to increase the pH of the injectate was shown not to be an effective approach due to the strong pH buffering effects of the native cation exchanger sites.

CFA and FAP are by far the most common phosphate minerals and are components of most rocks and sediments (Filippelli, 2002; Föllmi, 1996; Hughes, 2015; Hughes and Rakovan, 2015; Kholodov, 2014; Ruttenberg, 2003). Consequently, MAR projects which use RO-treated low ionic strength source water or source water that is low in calcium relative to the receiving aquifer should consider the risk of fluoride mobilisation from CFA or FAP and consider mitigating this risk by manipulating the AWT process with specific amendments. As the present study illustrates, the selection of an effective amendment and an appropriate amendment dose requires an advanced understanding of the geochemical conditions and prevailing mechanisms. Process-based reactive transport modelling showed to be a powerful interpretive tool to study the various options and to develop the mechanistic insights that are required in cases where several intertwined processes affect the aqueous concentrations of a groundwater constituent.

Declaration of Competing Interest

The authors declare that they have no known competing financial interests or personal relationships that could have appeared to influence the work reported in this paper.

Acknowledgements

D.S. was funded through a Robert and Maude Gledden scholarship from the University of Western Australia as well as a top-up scholarship from the National Centre for Groundwater Research and Training (NCGRT) and CSIRO Land and Water. H.P., J.S., and A.J.S. were all partially supported by the Water Corporation of Western Australia ("*Groundwater Replenishment Project Stages 3 and 4*" and "*Advanced Modelling Methodologies for Groundwater Resource Management and Asset Investment Planning*"), who also provided all required field as well as all required operational data.

References

Appelo, C.A.J., Postma, D., 2005. Geochemistry, Groundwater and Pollution. A.A. Balkema.
Atlas, E., Pytkowicz, R.M., 1977. Solubility Behavior of Apatites in Seawater. Limnol. Oceanogr. 22 (2), 290–300.
Atlas, E.L., 1975. Phosphate Equilibria in Seawater and Interstitial Waters. Oregon State University.
Betancourt, W.Q., Kitajima, M., Wing, A.D., Regnery, J., Drewes, J.E., Pepper, I.L., Gerba, C.P., 2014. Assessment of virus removal by managed aquifer recharge at three full-scale operations. Journal of Environmental Science and Health, Part A 49 (14), 8.
Birnhack, L., Voutchkov, N., Lahav, O., 2011. Fundamental chemistry and engineering aspects of post-treatment processes for desalinated water—A review. Desalination 273 (1), 6–22.

Borgnino, L., Garcia, M.G., Bia, G., Stupar, Y.V., Le Coustumer, P., Depetris, P.J., 2013. Mechanisms of fluoride release in sediments of Argentina's central region. Science of The Total Environment 443 (0), 245–255.
Brahman, K.D., Kazi, T.G., Afridi, H.I., Naseem, S., Arain, S.S., Ullah, N., 2013. Evaluation of high levels of fluoride, arsenic species and other physicochemical parameters in underground water of two sub districts of Tharparkar, Pakistan: a multivariate study. Water Res. 47 (3), 1005–1020.
Brown, C.J., Misut, P.E., 2010. Aquifer geochemistry at potential aquifer storage and recovery sites in coastal plain aquifers in the New York city area. USA. Applied Geochemistry 25 (9), 1431–1452.
Burris, D.L., 2018. Groundwater Replenishment System 2017 Annual Report. Orange County Water District.
Casanova, J., Devau, N., Pettenati, M., 2016. In: Jakeman, A.J., Barreteau, O., Hunt, R.J., Rinaudo, J.-D., Ross, A. (Eds.), Integrated Groundwater Management: concepts, Approaches and Challenges, Cham. Springer International Publishing, pp. 413–434.
Chaïrat, C., Oelkers, E.H., Schott, J., Lartigue, J.-.E., 2007a. Fluorapatite surface composition in aqueous solution deduced from potentiometric, electrokinetic, and solubility measurements, and spectroscopic observations. Geochim. Cosmochim. Acta 71 (24), 5888–5900.
Chaïrat, C., Schott, J., Oelkers, E.H., Lartigue, J.-.E., Harouiya, N., 2007b. Kinetics and mechanism of natural fluorapatite dissolution at 25 °C and pH from 3 to 12. Geochim. Cosmochim. Acta 71 (24), 5901–5912.
Christoffersen, J., Christoffersen, M.R., Johansen, T., 1996. Some new aspects of surface nucleation applied to the growth and dissolution of fluorapatite and hydroxyapatite. J Cryst Growth 163 (3), 304–310.
CSIRO and BOM, 2015. Climate Change in Australia Information For Australia's Natural Resource Management Regions. CSIRO and Bureau of Meteorology, Australia, p. 216.
CyMod_Systems, 2009. Perth Regional Aquifer Modelling System (PRAMS) Model development: Calibration of the Coupled Perth Regional Aquifer Model PRAMS 3.0. Report prepared by CyMod Systems Ptd Ltd, Department of Water, Western Australia.
CyMod_Systems, 2014. Construction and Calibration of the Perth Regional Aquifer Modelling System, PRAMS 3.5.2. Report prepared by CyMod Systems Pty Ltd, Department of Water, Western Australia.
Davidson, W.A., Yu, X., 2008. Perth Regional Aquifer Modelling System (PRAMS) Model Development. Department of Water, Perth, Western Australia.
Descourvieres, C., Douglas, G., Leyland, L., Hartog, N., Prommer, H., 2011. Geochemical reconstruction of the provenance, weathering and deposition of detrital–dominated sediments in the Perth Basin: the Cretaceous Leederville Formation, south-west Australia. Sediment. Geol. 236 (1–2), 62–76.
Descourvieres, C., Hartog, N., Patterson, B.M., Oldham, C., Prommer, H., 2010. Geochemical controls on sediment reactivity and buffering processes in a heterogeneous aquifer. Applied Geochemistry 25 (2), 261–275.
Dillon, P., 2005. Future management of aquifer recharge. Hydrogeol J 13 (1), 313–316.
Dillon, P., Stuyfzand, P., Grischek, T., Lluria, M., Pyne, R.D.G., Jain, R.C., Bear, J., Schwarz, J., Wang, W., Fernandez, E., Stefan, C., Pettenati, M., van der Gun, J., Sprenger, C., Massmann, G., Scanlon, B.R., Xanke, J., Jokela, P., Zheng, Y., Rossetto, R., Shamrukh, M., Pavelic, P., Murray, E., Ross, A., Bonilla Valverde, J.P., Palma Nava, A., Ansems, N., Posavec, K., Ha, K., Martin, R., Sapiano, M, 2018. Sixty years of global progress in managed aquifer recharge. Hydrogeol J.
DOE, 1997. In: Dickson, A.G., Goyet, C. (Eds.), Handbook of Methods For the Analysis of the Various Parameters of the Carbon Dioxide System in Sea Water. U.S. Department of Energy, p. 187 ORNL/CDIAC-74.
Donn, M.J., Patterson, B.M., Gerber, P., Prommer, H., 2017. Characterisation and Quantification of Water Quality Evolution During Recharge of Recycled Water Into the Yarragadee aquifer and the Leederville aquifer. CSIRO, p. 84.
Ebrahim, G.Y., Jonoski, A., Al-Maktoumi, A., Ahmed, M., Mynett, A., 2016. Simulation-Optimization Approach for Evaluating the Feasibility of Managed Aquifer Recharge in the Samail Lower Catchment. Oman. Journal of Water Resources Planning and Management 142 (2: 05015007), 16.
Eisenberg, T.N., Middlebrooks, E.J., 1985. Reverse Osmosis Treatment of Drinking Water. Elsevier Science, Cambridge, UNITED KINGDOM.
Fakhreddine, S., Dittmar, J., Phipps, D., Dadakis, J., Fendorf, S., 2015. Geochemical Triggers of Arsenic Mobilization during Managed Aquifer Recharge. Environ. Sci. Technol. 49 (13), 7802–7809.
Fakhreddine, S., Prommer, H., Gorelick, S.M., Dadakis, J., Fendorf, S., 2020. Controlling arsenic mobilization during managed aquifer recharge: the role of sediment heterogeneity. Environ. Sci. Technol. 54 (14), 8728–8738.
Fakhreddine, S., Prommer, H., Scanlon, B.R., Ying, S.C., Nicot, J.P., 2021. Mobilization of Arsenic and Other Naturally Occurring Contaminants during Managed Aquifer Recharge: A Critical Review. Environ Sci Technol 27. doi:10.1021/acs.est.0c07492, PMID: 33503373.
Feehley, C.E., Zheng, C., Molz, F.J., 2000. A dual-domain mass transfer approach for modeling solute transport in heterogeneous aquifers: application to the Macrodispersion Experiment (MADE) site. Water Resour Res 36 (9), 2501–2515.
Fienen, M.N. and Arshad, M. (2016) Integrated Groundwater Management: concepts, Approaches and Challenges. Jakeman, A.J., Barreteau, O., Hunt, R.J., Rinaudo, J.-D. and Ross, A. (eds), pp. 21-48, SpringerOpen.
Ganot, Y., Holtzman, R., Weisbrod, N., Russak, A., Katz, Y., Kurtzman, D, 2018. Geochemical processes during managed aquifer recharge with desalinated seawater. Water Resour Res 54 (2), 978–994.
Gibson, F.L., Burton, M., 2014. Salt or sludge? exploring preferences for potable water sources. Environmental and Resource Economics 57 (3), 24.
Gómez-Morales, J., Iafisco, M., Delgado-López, J.M., Sarda, S., Drouet, C., 2013. Progress on the preparation of nanocrystalline apatites and surface characterization: overview of fundamental and applied aspects. Progress in Crystal Growth and Characterization of Materials 59 (1), 1–46.
Guidry, M.W., Mackenzie, F.T., 2003. Experimental study of igneous and sedimentary apatite dissolution: control of pH, distance from equilibrium, and temperature on dissolution rates. Geochim. Cosmochim. Acta 67 (16), 2949–2963.
Händel, F., Fichtner, T.G., 2019. Numerical and Laboratory Investigations of Closely-Spaced and Joint Infiltration of Precipitation and Treated Waste Water. Water (Basel) 11 (2262), 17.
Henzler, A.F., Greskowiak, J., Massmann, G., 2014. Modeling the fate of organic micropollutants during river bank filtration (Berlin, Germany). J. Contam. Hydrol. 156, 78–92.
Higginson, S., Martin, M., 2012. Groundwater Replenishment Trial - Groundwater Report - 2012. Water Corporation, p. 135.
Jokela, P., Eskola, T., Heinonen, T., Tanttu, U., Tyrväinen, J., Artimo, A., 2017. Raw Water Quality and Pretreatment in Managed Aquifer Recharge for Drinking Water Production in Finland. Water (Basel) 9 (2), 16.
Jones, G.W., Pichler, T., 2007. Relationship between Pyrite Stability and Arsenic Mobility During Aquifer Storage and Recovery in Southwest Central Florida. Environ. Sci. Technol. 41 (3), 723–730.
Knappett, P.S.K., Li, Y., Loza, I., Hernandez, H., Aviles, M., Haaf, D., Majumder, S., Huang, Y., Lynch, B., Pina, V., Wang, J., Winkel, L., Mahlknecht, J., Datta, S., Thurston, W., Terrell, D., Kirk Nordstrom, D., 2020. Rising arsenic concentrations from dewatering a geothermally influenced aquifer in central Mexico. Water Res. 185, 116257 116257.
Kolehmainen, R.E., Langwaldt, J.H., Puhakka, J.A., 2007. Natural organic matter (NOM) removal and structural changes in the bacterial community during artificial groundwater recharge with humic lake water. Water Res. 41 (12), 11.
Kortelainen, N.M., Karhu, J.A., 2006. Tracing the decomposition of dissolved organic carbon in artificial groundwater recharge using carbon isotope ratios. Applied Geochemistry 21 (4), 6.
Leyland, L., 2011. Hydrogeology of the Leederville aquifer, Central Perth Basin, Western Australia. University of Western Australia.
McNab Jr, W.W., Singleton, M.J., Moran, J.E., Esser, B.K, 2009. Ion exchange and trace element surface complexation reactions associated with applied recharge of low-TDS water in the San Joaquin Valley. California. Applied Geochemistry 24 (1), 129–137.
Missimer, T.M., Maliva, R.G., Ghaffour, N., Leiknes, T., Amy, G.L., 2014. Economics for Wastewater Reuse in Low Population Wadi Communities, Kingdom of Saudi Arabia. Water (Basel) 6 (8), 17.
Moscovis, V., 2013. Groundwater Replenishment Trial - Final Report. Water Corporation, p. 193.
Ormerod, K.J., 2015. Governing risk, reuse, and reclamation: water pollution control and new water resources in the southwestern united states The University of Arizona. Available from ProQuest Dissertations & Theses Global.
Parkhurst, D.L., 2015. PHREEQC (Version 3)–A Computer Program For Speciation, Batch-Reaction, One-Dimensional Transport, and Inverse Geochemical Calculations. US Geological Survey.
Pham, V.T.H., Lu, P., Aagaard, P., Zhu, C., Hellevang, H, 2011. On the potential of CO2–water–rock interactions for CO2 storage using a modified kinetic model. International Journal of Greenhouse Gas Control 5 (4), 1002–1015.
Prommer, H., Sun, J., Helm, L., Rathi, B., Siade, A.J., Morris, R., 2018. Deoxygenation Prevents Arsenic Mobilization during Deepwell Injection into Sulfide-Bearing Aquifers. Environ. Sci. Technol. 52 (23), 10.
Rathi, B., Siade, A.J., Donn, M.J., Helm, L., Morris, R., Davis, J.A., Berg, M., Prommer, H., 2017. Multiscale Characterization and Quantification of Arsenic Mobilization and Attenuation During Injection of Treated Coal Seam Gas Co-produced Water into Deep Aquifers. Water Resour Res 53 (12), 10779–10801.
Reichard, E.G., Johnson, T.A., 2005. Assessment of Regional Management Strategies for Controlling Seawater Intrusion. Journal of Water Resources Planning and Management 131 (4), 280–291.
Richards, L.A., Richards, B.S., Schäfer, A.I., 2011. Renewable energy powered membrane technology: salt and inorganic contaminant removal by nanofiltration/reverse osmosis. J Memb Sci 369 (1), 188–195.
Rodriguez, C., Van Buynder, P., Lugg, R., Blair, P., Devine, B., Cook, A., Weinstein, P., 2009. Indirect Potable Reuse: a Sustainable Water Supply Alternative. Int J Environ Res Public Health 6 (3), 1174.
Sazakli, E., Alexopoulos, A., Leotsinidis, M., 2007. Rainwater harvesting, quality assessment and utilization in Kefalonia Island. Greece. Water Research 41 (9), 2039–2047.
Schafer, D., Donn, M., Atteia, O., Sun, J., Macrae, C., Raven, M., Pejcic, B., Prommer, H., 2018. Fluoride and phosphate release from carbonate-rich fluorapatite during managed aquifer recharge. J Hydrol (Amst) 562, 809–820.
Schafer, D., Sun, J., Jamieson, J., Siade, A.J., Atteia, O., Prommer, H., 2020. Model-Based Analysis of Reactive Transport Processes Governing Fluoride and Phosphate Release and Attenuation during Managed Aquifer Recharge. Environ. Sci. Technol. 54 (5), 2800–2811.
Schweizer, D., Prommer, H., Blum, P., Siade, A.J., Butscher, C., 2018. Reactive transport modeling of swelling processes in clay-sulfate rocks. Water Resour Res 54 (9), 6543–6565.
Seibert, S., Atteia, O., Salmon, S.U., Siade, A., Douglas, G., Prommer, H., 2016. Identification and quantification of redox and pH buffering processes in a hetero-

geneous, low carbonate aquifer during managed aquifer recharge. Water Resour Res 52 (5), 4003–4025.
Seibert, S., Prommer, H., Siade, A., Harris, B., Trefry, M., Martin, M., 2014. Heat and mass transport during a groundwater replenishment trial in a highly heterogeneous aquifer. Water Resour Res 50 (12), 9463–9483.
Siade, A.J., Cui, T., Karelse, R.N., Hampton, C., 2020. Reduced-Dimensional Gaussian Process Machine Learning for Groundwater Allocation Planning using Swarm Theory. Water Resurces Research 56, e2019WR026061.
Siade, A.J., Hall, J., Karalse, R.N., 2017. A practical, robust methodology for acquiring new observation data using computationally expensive groundwater models. Water Resour Res 53 (11), 9860–9882.
Sidhu, J.P.S., Toze, S., Hodgers, L., Barry, K., Page, D., Li, Y., Dillon, P, 2015. Pathogen Decay during Managed Aquifer Recharge at Four Sites with Different Geochemical Characteristics and Recharge Water Sources. J. Environ. Qual. 44 (5), 11.
Starr, J.L., Parlange, J.-.Y., 1979. Dispersion in soil columns: the Snow Plough Effect. Soil Science Society of America Journal 43 (3), 448–450.
Stefan, C., Ansems, N., 2018. Web-based global inventory of managed aquifer recharge applications. Sustain Water Resour Manag 4 (2), 10.
Stuyfzand, P., Smidt, E., Zuurbier, K., Hartog, N., Dawoud, M., 2017. Observations and prediction of recovered quality of desalinated seawater in the strategic ASR project in Liwa. Abu Dhabi. Water 9 (3), 177.
Sun, J., Donn, M.J., Gerber, P., Higginson, S., Siade, A.J., Schafer, D., Seibert, S., Prommer, H., 2020. Assessing and Managing Large-Scale Geochemical Impacts from Groundwater Replenishment with Highly Treated Reclaimed Wastewater. Water Resour Res 56, e2020WR028066.
Tang, Z., Hong, S., Xiao, W., Seal, S., T., J., 2006a. Effect of varying blends of finished RO, surface and ground waters on solid lead surfaces. Corros Sci 48, 3413–3427.
Tang, Z., Hong, S., Xiao, W., Taylor, J., 2006b. Impacts of blending ground, surface, and saline waters on lead release in drinking water distribution systems. Water Res. 40, 943–950.
Timms, N.E., Olierook, H.K.H., Wilson, M.E.J., Piane, C.D., Hamilton, P.J., Cope, P., Stütenbecker, L, 2015. Sedimentary facies analysis, mineralogy and diagenesis of the Mesozoic aquifers of the central Perth Basin, Western Australia. Mar Pet Geol 60 (0), 54–78.
Treumann, S., Torkzaban, S., Bradford, S.A., Visalakshan, R.M., Page, D, 2014. An explanation for differences in the process of colloid adsorption in batch and column studies. J. Contam. Hydrol. 164 (0), 219–229.
Tribble, J.S., Arvidson, R.S., Lane, M., Mackenzie, F.T., 1995. Crystal chemistry, and thermodynamic and kinetic properties of calcite, dolomite, apatite, and biogenic silica: applications to petrologic problems. Sediment. Geol. 95 (1–2), 11–37.
Underwood, S.C., McCallum, J.L., Cook, P.G., Simmons, C.T., Dogramaci, S., Purtschert, R., Siade, A.J., Prommer, H., 2018. Physical and Chemical Controls on the Simultaneous Occurrence of Young and Old Groundwater Inferred From Multiple Age Tracers. Water Resour Res 54 (11), 9514–9532.
UNESCO, 2016. Water and Jobs - The United Nations World Development Report 2016. United Nations Educational, Scientific and Cultural Organisation, Paris, p. 148.
Vandenbohede, A., Wallis, I., Van Houtte, E., Van Ranst, E., 2013. Hydrogeochemical transport modeling of the infiltration of tertiary treated wastewater in a dune area. Belgium. Hydrogeology Journal 21 (6), 1307–1321.
Wallis, I., Prommer, H., Simmons, C.T., Post, V., Stuyfzand, P.J., 2010. Evaluation of Conceptual and Numerical Models for Arsenic Mobilization and Attenuation during Managed Aquifer Recharge. Environ. Sci. Technol. 44 (13), 5035–5041.
Wester, J., Timpano, K.R., Cek, D., Lieberman, D., Fieldstone, S.C., Broad, K., 2015. Psychological and social factors associated with wastewater reuse emotional discomfort. J Environ Psychol 42, 8.
Wester, J.N., 2016. Morality, emotion, and Policy making: Environmental decision Making About Recycled Water. University of Miami, ProQuest Dissertations Publishing.
WHO, 2017. Guidelines For Drinking-water quality - fourth edition Incorporating the First Addendum. World Health Organization, p. 541.
Wiese, B., Massmann, G., Jekel, M., Heberer, T., Dünnbier, U., Orlikowski, D., Grützmacher, G., 2011. Removal kinetics of organic compounds and sum parameters under field conditions for managed aquifer recharge. Water Res. 45 (16), 12.
Yu, X., Chen, J., Li, Y., Liu, H., Hou, C., Zeng, Q., Cui, Y., Zhao, L., Li, P., Zhou, Z., Pang, S., Tang, S., Tian, K., Zhao, Q., Dong, L., Xu, C., Zhang, X., Zhang, S., Liu, L., Wang, A., 2018. Threshold effects of moderately excessive fluoride exposure on children's health: a potential association between dental fluorosis and loss of excellent intelligence. Environ Int 118, 9.
Yuan, J., Van Dyke, M.I., Huck, P.M., 2019. Selection and evaluation of water pretreatment technologies for managed aquifer recharge (MAR) with reclaimed water. Chemosphere 236, 15 (December 2019, 124886).
Zekri, S., Ahmed, M., Chaieb, R., Ghaffour, N., 2014. Managed aquifer recharge using quaternary-treated wastewater: an economic perspective. International Journal of Water Resources Development 30 (2), 16.